Atmospheric Forcing of the Pacific Meridional Mode: Tropical Pacific-Driven Versus Internal Variability

Yu Zhang[1,2] [ID]**, Shi-Yun Yu[1,3]** [ID]**, Dillon J. Amaya[4]** [ID]**, Yu Kosaka[5]** [ID]**, Malte F. Stuecker[6], Jun-Chao Yang[1,2], Xiaopei Lin[1,2]** [ID]**, and Lei Fan[1,3]** [ID]

[1]Frontier Science Center for Deep Ocean Multispheres and Earth System (FDOMES) and Physical Oceanography Laboratory, Ocean University of China, Qingdao, China, [2]Qingdao National Laboratory for Marine Science and Technology, Qingdao, China, [3]College of Oceanic and Atmospheric Sciences, Ocean University of China, Qingdao, China, [4]Physical Science Laboratory, Earth System Research Laboratory, National Oceanic and Atmospheric Administration, Boulder, CO, USA, [5]Research Center for Advanced Science and Technology, The University of Tokyo, Tokyo, Japan, [6]Department of Oceanography and International Pacific Research Center, School of Ocean and Earth Science and Technology, University of Hawai'i at Mānoa, Honolulu, Hawai'i

Abstract The Pacific Meridional Mode (PMM) impacts tropical Pacific sea surface temperature variations, which in turn affect the PMM through the excited atmospheric teleconnections. Previous studies linked this loop to the tropical Pacific-excited North Pacific Oscillation (NPO; the second empirical mode of North Pacific sea level pressure variability), while a recent study proposed the linkage to the excited Aleutian low (AL) variability (the first empirical mode). Unraveling their relative importance for the loop is thus crucial for better understanding subtropical-tropical interactions. Here, using tropical Pacific pacemaker experiments we show that tropical Pacific-forced AL variability is tied to the loop, while the tropical Pacific-forced NPO does not effectively induce PMM variability, hence not being in the loop. Our study emphasizes the role of tropical Pacific-forced AL variability in the PMM-tropical Pacific interaction, which should be paid more attention in future studies.

Plain Language Summary The Pacific Meridional Mode (PMM) is a prominent pattern of climate variability situated in the subtropical northeastern Pacific. Sea surface temperature (SST) anomalies associated with the PMM can propagate into the deep tropics via a feedback process involving the coupling between wind, evaporation, and SST. In the tropics, these SST anomalies can induce a response of the extratropical atmospheric circulation—so-called teleconnections—which in turn can induce PMM variability via the effect of this anomalous atmospheric circulation on surface heat fluxes in the subtropics. Previous studies linked the tropical-to-subtropical teleconnection in this loop to the second leading statistical pattern of North Pacific atmospheric variability—the so-called North Pacific Oscillation. However, a recent study pointed out that this tropical-to-subtropical teleconnection is also associated with prominent anomalies of the Aleutian low (AL)—the first leading statistical pattern of North Pacific atmospheric variability. To reveal which dominant pattern of atmospheric variability is primarily tied to the teleconnection, we quantify their relative role in causing PMM variability based on climate model simulations. We find that AL variability plays the key role in linking the tropics with the subtropics.

1. Introduction

The Pacific Meridional Mode (PMM) is the leading ocean-atmosphere coupled mode between sea surface temperature (SST) and surface wind anomalies over the subtropical northeastern Pacific (Amaya, 2019; Chiang & Vimont, 2004). Part of its variability is simultaneously independent of the El Niño-Southern Oscillation (ENSO; Chiang & Vimont, 2004), but it can affect ENSO through multiple atmosphere-ocean thermodynamic and dynamic coupled processes (Amaya, 2019; Amaya et al., 2019; Larson & Kirtman, 2013). Therefore, further investigating the formation mechanism of the PMM might benefit our understanding of tropical Pacific variability (Liguori & Di Lorenzo, 2018; Yang et al., 2021).

SST variability associated with the PMM is suggested to be mainly initiated by North Pacific atmospheric forcing (Chiang & Vimont, 2004). Specifically, North Pacific atmospheric variability affects the strength of the northeasterly trade winds, altering latent heat flux exchange between the ocean and atmosphere, and therefore inducing the PMM through a process called wind-evaporation-SST (WES) feedback (Xie & Philander, 1994).

Previous studies have shown that the leading atmospheric driver of changes in trade wind strength is related to the North Pacific Oscillation (NPO; Rogers, 1981; Walker & Bliss, 1932), which is the second empirical orthogonal function (EOF) mode of sea level pressure (SLP) variability over the North Pacific. Its southern lobe over the Hawaiian Islands can effectively initiate the WES feedback and thus the PMM (Chiang & Vimont, 2004; Zhang et al., 2021). In addition to the NPO, a recent study by Zhang et al. (2021) identified a new North Pacific atmospheric mode contributing to forcing the PMM, termed the North Pacific Tripole (NPT), which emerges as the fourth SLP EOF mode. Its forcing role is attributed to the center of action over the west coast of North America, which impacts trade winds strength and can also initiate the WES feedback.

After the PMM is initiated, it can impact tropical Pacific SSTs (Amaya, 2019; Amaya et al., 2019), which excite poleward atmospheric teleconnections (Alexander et al., 2002), further influencing PMM variability through the WES feedback. These processes form an interaction between the PMM and tropical Pacific SST variability. Previous studies mostly attributed the interaction process to the tropical Pacific-forced NPO variability (the second EOF mode of North Pacific SLP variability; Di Lorenzo et al., 2010; Furtado et al., 2012; Di Lorenzo et al., 2015), while a recent study by Stuecker (2018) additionally linked the process to tropical Pacific-forced Aleutian low (AL) fluctuations (the first EOF mode of North Pacific SLP variability), whose associated wind variability on its southern flank is able to affect trade winds strength, thereby driving PMM variability. The debate on the relative roles of tropical Pacific-forced NPO and AL variability in bridging the PMM and tropical Pacific SST variations needs to be revealed.

To untangle these different physical mechanisms, we use tropical Pacific pacemaker experiments to dynamically separate tropical Pacific-forced and internal (i.e., independent of tropical Pacific forcing) components of North Pacific atmospheric variability and investigate their individual roles in forcing the PMM. Our analyses showed that tropical Pacific-forced AL variability contributes to driving the PMM, whereas tropical Pacific-forced NPO variability is not effective. Therefore, our study implies a key role of tropical Pacific-forced AL in linking the PMM and tropical Pacific variability, rather than tropical Pacific-forced NPO variability that was proposed in most prior studies.

2. Data and Methods

2.1. Observational Data

Before separating tropical Pacific-forced and internal variability based on tropical Pacific pacemaker experiments, we first used observational data to examine the roles of leading modes of North Pacific SLP variability in forcing the PMM. We used monthly SST data from the NOAA Extended Reconstructed SST version 5 (ERSSTv5) with a horizontal resolution of 2° longitude × 2° latitude (Huang et al., 2017). We also used atmospheric reanalysis data of monthly SLP and 10-m wind from the NOAA-CIRES-DOE Twentieth Century Reanalysis version 3 (20CRv3) with a horizontal resolution of 1° longitude × 1° latitude (Slivinski et al., 2019). The time periods of the two datasets used are both from 1900 to 2014. We analyzed monthly anomalies of all variables obtained by removing the monthly 1900–2014 climatology and the linear trend.

2.2. Tropical Pacific Pacemaker Experiments

To further investigate the roles of tropical Pacific SST-driven and internal variability of North Pacific SLP leading atmospheric circulation modes in forcing the PMM, we used a tropical Pacific pacemaker experiment—Pacific Ocean-Global Atmosphere (POGA; Kosaka & Xie, 2013, 2016; Yang et al., 2020; Zhang et al., 2018)—based on the Geophysical Fluid Dynamics Laboratory Coupled Model version 2.1 (CM2.1; Delworth et al., 2006). The POGA simulation consists of 10 ensemble members; each member was forced by identical observed SST anomalies in the tropical eastern Pacific (from 180° to the American west coast, 15°S–15°N, with a 5° buffer zone north, south, and west of the domain) as well as CMIP5 historical and representative concentration pathway 4.5 (RCP4.5) radiative forcing from 1861 to 2014, but with slightly different atmosphere-ocean initial conditions. To remove the effect of radiative forcing, we used a 20-member ensemble of CM2.1 historical simulations, each forced by historical and RCP4.5 radiative forcing and different initial conditions. The tropical Pacific-forced component is therefore obtained by subtracting the ensemble mean of the historical experiments from the ensemble mean of the POGA simulations; whereas internal variability is obtained by subtracting the ensemble mean of

the POGA simulations from each POGA member. To be consistent with the observations, we also analyzed the POGA simulations from 1900 to 2014.

To examine the robustness of the results from the CM2.1 POGA, we also analyzed another POGA experiment with its historical simulation based on the Community Earth System Model version 1.1 (CESM; Deser et al., 2017). We used 10 ensemble members of CESM POGA with 40-member historical simulations from 1920 to 2013. The results based on the CESM POGA are presented in Supporting Information.

2.3. A First-Order Autoregressive Model

To determine whether leading EOF modes of North Pacific SLP variability can significantly drive PMM variability, we reconstructed SST indices forced by these SLP variabilities based on a first-order autoregressive model (AR-1) following Di Lorenzo and Mantua (2016):

$$\frac{dSST(t)}{dt} = \alpha SLP(t) - \frac{SST(t)}{\tau}, \tag{1}$$

where $SST(t)$ is the normalized reconstructed monthly SST index; $SLP(t)$ is the normalized monthly principal component (PC) of SLP variability derived from the EOF analysis of monthly SLP anomalies over the North Pacific (10°–80°N, 130°E−110°W); in this study, we only analyzed the first four SLP EOF modes—AL, NPO, the third EOF mode, and NPT—which were mutually well separated based on North's rule (North et al., 1982); the reason we used their monthly PCs is that in both observations and the POGA experiments, while their variabilities are strongest in boreal winter (Figure S1), they exhibit variance throughout the whole year; dt is a time step of 1 month; α is a scaling factor associated with the forcing term, which is 1 mon^{-1}; τ is an e-folding timescale of 9 months, estimated from the decorrelation timescale of the PMM index (time at which the autocorrelation drops to $1/e$; slightly changing the value of τ does not affect the conclusions drawn in this study). The PMM index is represented by the SST expansion coefficient derived from a singular value decomposition (SVD) analysis between SST and 10-m wind anomalies over the subtropical northeastern Pacific (10°–30°N, 160°E−100°W) after linearly removing the cold tongue index month-by-month, the procedure following Zhang et al. (2021). If the reconstructed SST and the PMM indices are significantly correlated, then it suggests that the leading North Pacific SLP mode used to reconstruct the SST index contributes to forcing the PMM.

### 2.4. Effective Degree of Freedom

Effective sample size N^* was estimated using the modified Chelton method (Ding et al., 2015; Pyper & Peterman, 1998) and can be obtained from a theoretical approximation:

$$N^* \approx \frac{N}{1 + 2 \sum_{i=1}^{N} \frac{N-i}{N} R_X(i) R_Y(i)}, \tag{2}$$

where N is the sample size; $R_X(i)$ and $R_Y(i)$ are the autocorrelations of the two sampled time series $X(i)$ and $Y(i)$, respectively. The effective degree of freedom is thus the effective sample size minus 2. Two-tailed Student's t-test and F-test were used for statistically testing correlation and regression analyses, respectively.

3. Results

We first examine the two POGAs' skills in simulating the observed spatial patterns of the leading North Pacific SLP modes and their roles in forcing the PMM. The spatial patterns are displayed as regressions of monthly SLP anomalies against the respective normalized SLP PC (contours in Figures 1 and S3). The patterns are overlaid with simultaneously regressed monthly 10-m wind (vectors in Figures 1 and S3) and lag-1-month SST (shading in Figures 1 and S3) anomalies, the latter of which is given by an approximate lag-1-month relationship between the SLP variabilities and PMM SSTs in both observations and POGA experiments (Fig. S2). The forcing roles of the SLP variabilities in the PMM are measured by the correlations between the reconstructed SST index based on the AR-1 model and PMM index (right columns in Figures 1 and S3).
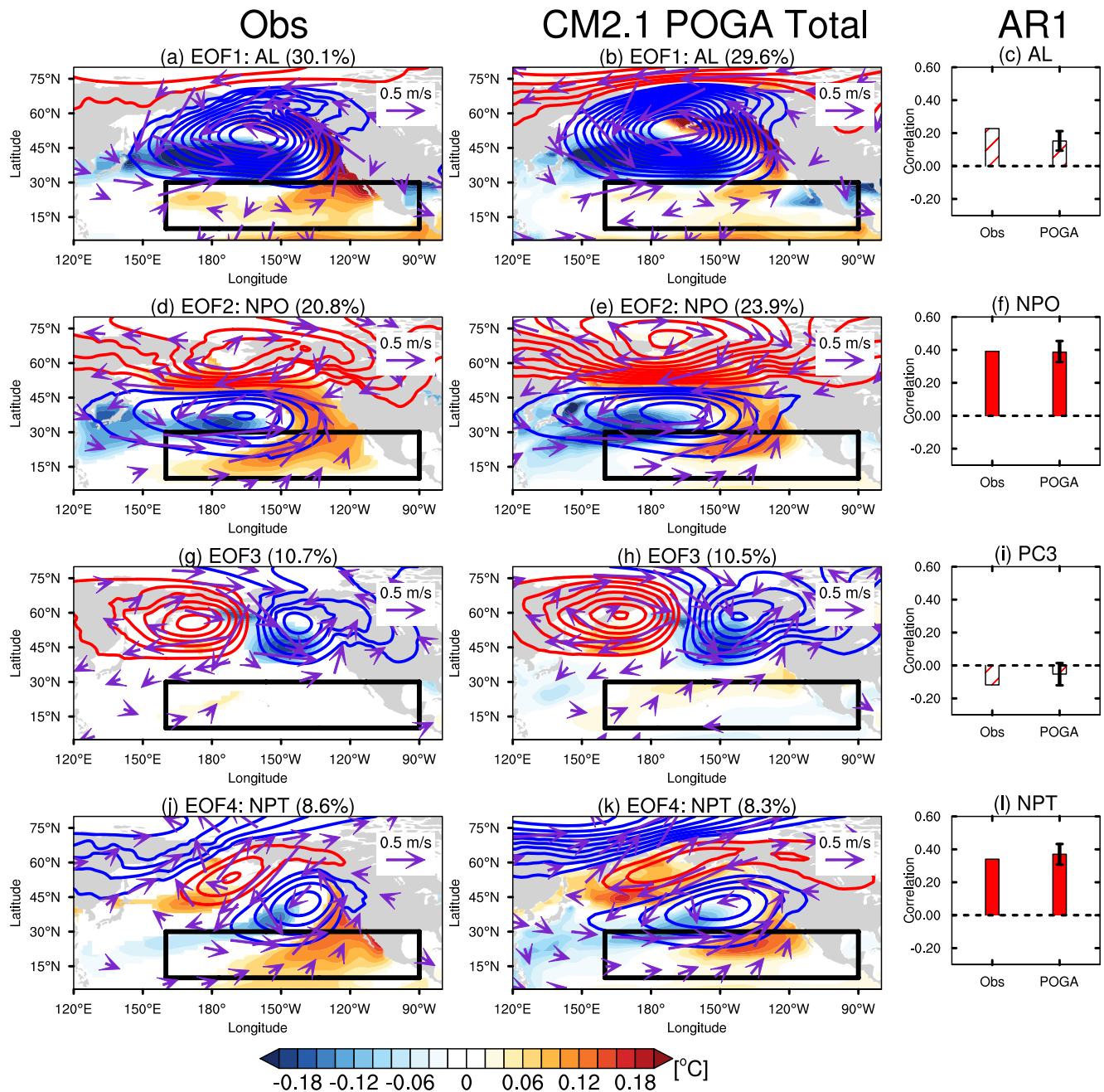
Figure 1. (left and middle columns) The first four empirical orthogonal function (EOF) modes of North Pacific monthly sea level pressure (SLP) anomalies and (right column) correlations of the Pacific Meridional Mode (PMM) index with the SLP reconstructed SST indices based on the AR-1 model in observations and the CM2.1 Pacific Ocean-Global Atmosphere (POGA). Patterns are shown as the regressed monthly SLP (contour interval: 0.5 hPa; red for positive and blue for negative), 10-m wind (vectors; m s^{-1}), and lag-1-month SST (°C) anomalies against normalized monthly SLP PC. Only the regression coefficients exceeding the 99% confidence level are shown, except for the SLP field, which is presented as a whole pattern for clarity. The explained variance of each SLP mode is marked in the title of each panel. Black box denotes the PMM SVD domain. In the right column, red bars (bars with red slash) denote the correlations statistically significant (insignificant) at the 99% confidence level. The bars (error bars) for the CM2.1 POGA denotes the mean (1 standard deviation) of the correlations of the CM2.1 POGA members.

The results show that, overall, the two POGAs well capture both the pattern and forcing role of the leading SLP variabilities in the PMM (Figures 1 and S3). Specifically for the latter, the POGAs capture the less effective forcing role of AL variability in the PMM (Figures 1c and S3c). In addition, POGA results show the significant forcing roles of NPO and NPT variabilities in the PMM (Figures 1f, 1l and S3f, S3l), consistent with previous findings (Amaya, 2019; Chiang & Vimont, 2004; Zhang et al., 2021). All the above results are significant at the
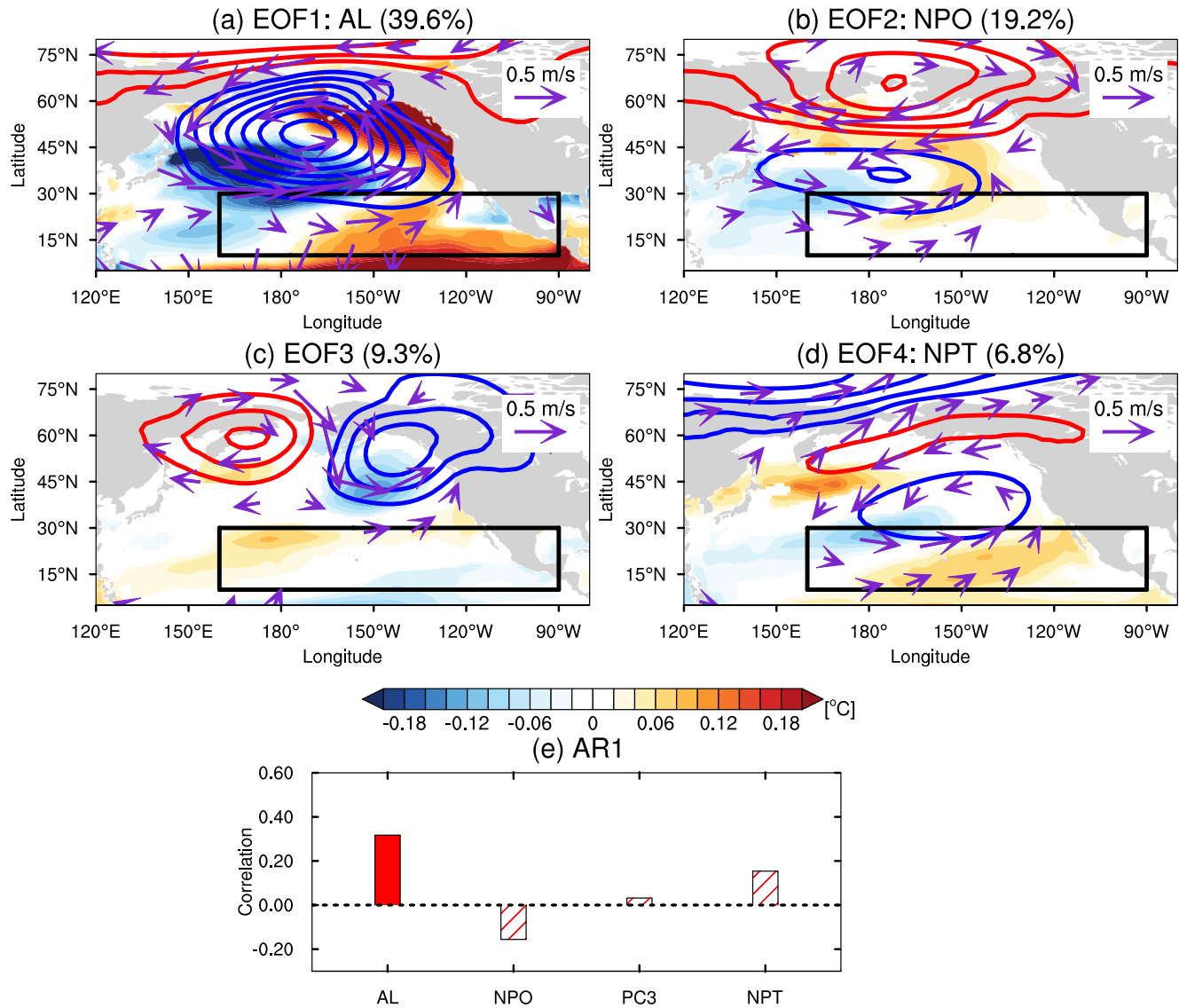
Figure 2. As in Figure 1, but for the tropical Pacific-forced variability in the CM2.1 Pacific Ocean-Global Atmosphere (POGA).

99% confidence level. In all, the POGA simulation's skill provides a basis for further investigating the roles of tropical Pacific-forced and internal components of the leading SLP modes in forcing the PMM.

Next, we investigate the roles of tropical Pacific-forced North Pacific SLP variability in forcing the observed PMM (Figures 2 and S4). To obtain the leading modes of variability, we perform the EOF analysis on monthly SLP anomalies over the North Pacific for the POGA ensemble mean. The results show that the tropical Pacific-forced AL variability is able to force the PMM (Figures 2e and S4e). This is attributed to its spatial pattern with the southward shifted cyclonic circulation (Figures 2a and S4a), which affects trade wind strength and thus forces the PMM through WES feedback. The pattern and forcing role associated with the tropical Pacific-forced AL variability are consistent with the finding by Stuecker (2018). Additionally, it is noted that this southward shifted AL pattern in both POGA experiments is not seen in observations, the latter of which shows more eastward displacement associated with the SST variability in the POGA restoring region (Figure S5). This distinction might be attributed to the statistical method that cannot dynamically isolate the tropical Pacific-forced variability in observations. For the tropical Pacific-forced NPO and NPT (Figures 2b, 2d and S4b, S4c; note that the NPT

CM2.1 POGA Internal
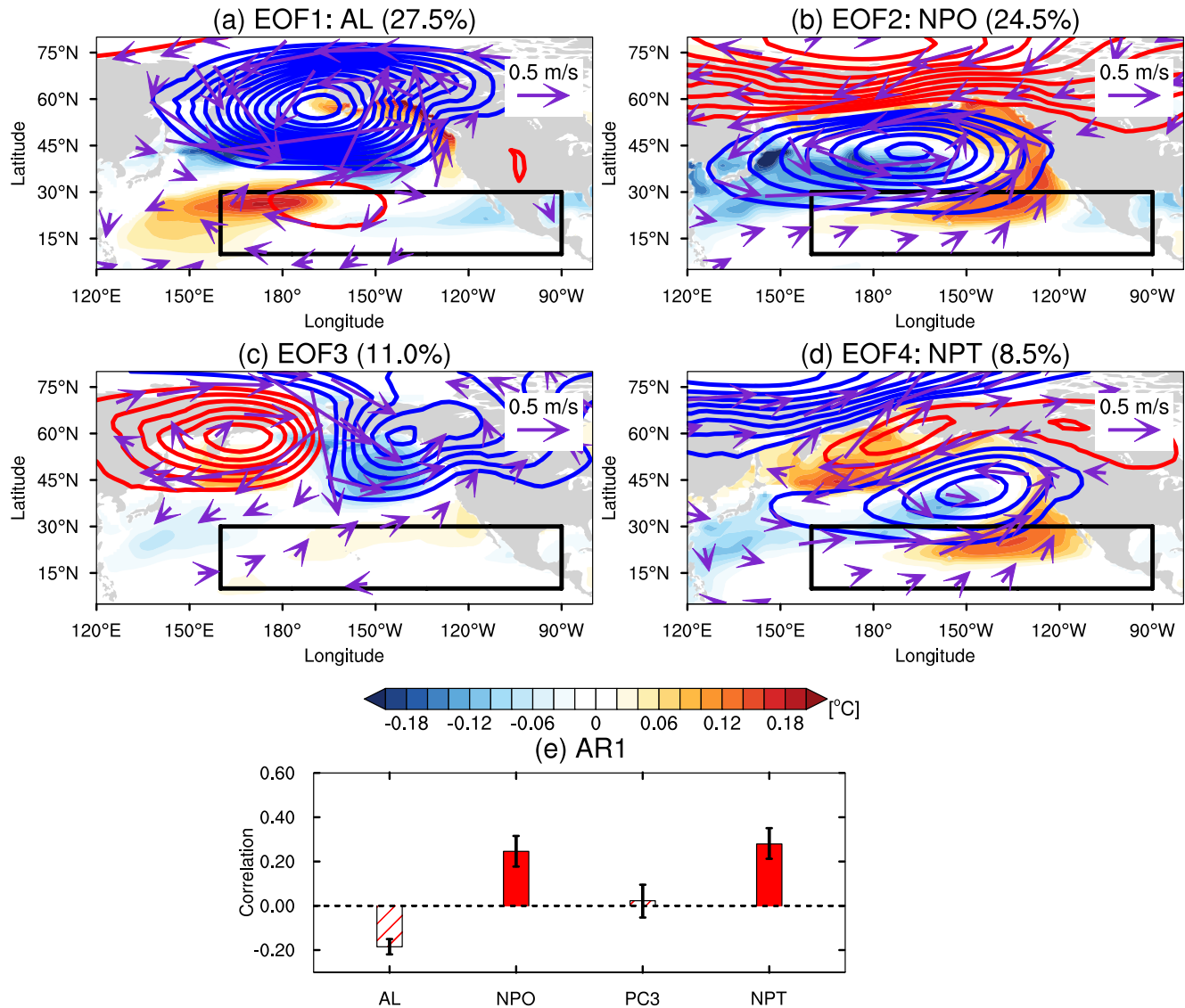
Figure 3. As in Figure 2, but for the internal variability in the CM2.1 Pacific Ocean-Global Atmosphere (POGA).

in the CESM POGA ensemble mean emerges as the third EOF mode), although they can relax the trade winds, they do not significantly contribute to forcing the PMM (Figures 2e and S4e). This is because their amplitudes are smaller than their internal counterparts (Figures 3b, 3d and S6b, S6d), resulting in the less contributions to forcing the PMM.

Last, we explore the roles of internal variability of these leading SLP modes in forcing the PMM in the two POGA experiments (Figures 3 and S6). To obtain these internal variabilities, we perform the EOF analysis on monthly SLP anomalies of concatenated POGA ensemble members over the North Pacific after subtracting the ensemble mean. By this procedure, each mode has only one EOF pattern and PC across POGA members. We then use each PC to reconstruct an SST index based on the AR-1 model and correlate it with the PMM index in each POGA member. The mean of the correlations (statistically tested) with ±1 standard deviation is presented (Figures 3e and S6e).

The results show that, for internal AL variability, the anomalous cyclonic circulation is located further northward, far away from the subtropics, hence hardly affecting the trade winds and driving the PMM in both POGAs
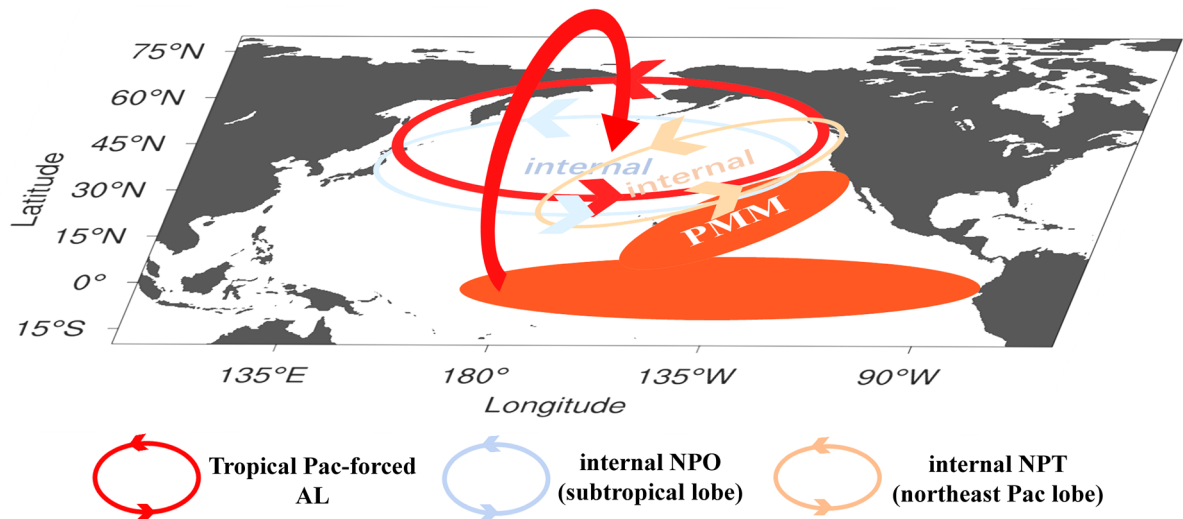
Figure 4. Schematic of the North Pacific atmospheric forcing of the Pacific Meridional Mode (PMM).

(Figures 3a and S6a). In addition to the northward displaced cyclonic circulation, there is a weak anticyclonic circulation evident over the subtropics in the CM2.1 POGA (Figure 3a). The presence of this anticyclonic circulation may arise from wave-mean flow interaction pointed out by Chen et al. (2020), in which they showed that AL variability in March that is mostly independent of pre-winter ENSO events features anomalously high pressure south of the AL as a result of wave-mean flow interaction. This anomalous anticyclonic circulation will reverse the forcing role by the cyclonic circulation (negative correlation in Figure 3e). Since the internal AL variability is stronger than the tropical Pacific-forced counterpart (compare Figures 2a and S4a to Figures 3a and S6a), its less effective forcing role explains the forcing role of observed AL variability in the PMM (Figures 1c and S3c). For the internal NPO and NPT variabilities (Figures 3b, 3d and S6b, S6d), as aforementioned, because their magnitudes are stronger than the tropical Pacific-forced counterparts (Figures 2b, 2d and S4b, S4c), they contribute to forcing the PMM (Figures 3e and S6e).

4. Summary

We have used the CM2.1 and CESM POGA experiments to investigate the relative roles of both tropical Pacific-forced and internal variability of the leading North Pacific SLP modes in forcing the PMM (the main findings are summarized in Figure 4). Specifically, the center of action of tropical Pacific-forced AL variability is located more southward than the spatial pattern of internal AL variability, therefore affecting trade winds strength and forcing the PMM effectively. In contrast, the center of action of internal AL variability is located in the North Pacific midlatitudes, far away from the subtropics, thus being inconducive to forcing the PMM. For NPO and NPT variabilities, while their tropical Pacific-forced variability is able to affect trade wind strength, their internal variability is much stronger than their tropical Pacific-forced variability, leading to effective forcing patterns for the PMM. Among the tropical Pacific-forced components of the four leading statistical modes of North Pacific atmospheric variability, only tropical Pacific-excited AL variability contributes effectively to forcing the PMM. Hence, it plays a key role in linking PMM and tropical Pacific variability.

Data Availability Statement

References

Alexander, M. A., Bladé, I., Newman, M., Lanzante, J. R., Lau, N. C., & Scott, J. D. (2002). The atmospheric bridge: The influence of ENSO teleconnections on air–sea interaction over the global oceans. *Journal of Climate*, *15*(16), 2205–2231. https://doi.org/10.1175/1520-0442(2002)015<2205:TABTIO>2.0.CO;2

Amaya, D. J. (2019). The Pacific meridional mode and ENSO: A review. *Current Climate Change Reports*, *5*, 296–307. https://doi.org/10.1007/s40641-019-00142-x

Amaya, D. J., Kosaka, Y., Zhou, W., Zhang, Y., Xie, S.-P., & Miller, A. J. (2019). The North Pacific pacemaker effect on historical ENSO and its mechanisms. *Journal of Climate*, *32*, 7643–7661. https://doi.org/10.1175/jcli-d-19-0040.1

Chen, S., Chen, W., Wu, R., Yu, B., & Graf, H. F. (2020). Potential impact of preceding Aleutian low variation on El Niño–Southern oscillation during the following winter. *Journal of Climate*, *33*(8), 3061–3077. https://doi.org/10.1175/JCLI-D-19-0717.1

Chiang, J., & Vimont, D. J. (2004). Analogous Pacific and Atlantic meridional modes of tropical atmosphere–ocean variability. *Journal of Climate*, *17*, 4143–4158. https://doi.org/10.1175/jcli4953.1

Delworth, T. L., Broccoli, A. J., Rosati, A., Stouffer, R. J., Balaji, V., Beesley, J. A., et al. (2006). GFDL's CM2 global coupled climate models. Part I: Formulation and simulation characteristics. *Journal of Climate*, *13*, 643–674. https://doi.org/10.1175/jcli3629.1

Deser, C., Guo, R., & Lehner, F. (2017). The relative contributions of tropical Pacific sea surface temperatures and atmospheric internal variability to the recent global warming hiatus. *Geophysical Research Letters*, *44*, 7945–7954. https://doi.org/10.1002/2017gl074273

Di Lorenzo, E., Cobb, K. M., Furtado, J. C., Schneider, N., Anderson, B. T., Bracco, A., et al. (2010). Central Pacific El Niño and decadal climate change in the North Pacific ocean. *Nature Geoscience*, *3*(11), 762–765. https://doi.org/10.1038/ngeo984

Di Lorenzo, E., Liguori, G., Schneider, N., Furtado, J. C., Anderson, B. T., & Alexander, M. A. (2015). ENSO and meridional modes: A null hypothesis for Pacific climate variability. *Geophysical Research Letters*, *42*(21), 9440–9448. https://doi.org/10.1002/2015GL066281

Di Lorenzo, E., & Mantua, N. (2016). Multi-year persistence of the 2014/15 North Pacific marine heatwave. *Nature Climate Change*, *6*(11), 1042–1047. https://doi.org/10.1038/nclimate3082

Ding, R., Li, J., & Tseng, Y. H. (2015). The impact of South Pacific extratropical forcing on ENSO and comparisons with the North Pacific. *Climate Dynamics*, *44*(7–8), 2017–2034. https://doi.org/10.1007/s00382-014-2303-5

Furtado, J. C., Di Lorenzo, E., Anderson, B. T., & Schneider, N. (2012). Linkages between the North Pacific Oscillation and central tropical Pacific SSTs at low frequencies. *Climate Dynamics*, *39*(12), 2833–2846. https://doi.org/10.1007/s00382-011-1245-4

Huang, B., Thorne, P. W., Banzon, V. F., Boyer, T., Chepurin, G., Lawrimore, J. H., et al. (2017). Extended reconstructed sea surface temperature, version 5 (ERSSTv5): Upgrades, validations, and intercomparisons. *Journal of Climate*, *30*(20), 8179–8205. https://doi.org/10.1175/JCLI-D-16-0836.1

Kosaka, Y., & Xie, S.-P. (2013). Recent global-warming hiatus tied to equatorial Pacific surface cooling. *Nature*, *501*, 403–407. https://doi.org/10.1038/nature12534

Kosaka, Y., & Xie, S.-P. (2016). The tropical Pacific as a key pacemaker of the variable rates of global warming. *Nature Geoscience*, *9*, 669–673. https://doi.org/10.1038/ngeo2770

Larson, S., & Kirtman, B. (2013). The Pacific Meridional Mode as a trigger for ENSO in a high-resolution coupled model. *Geophysical Research Letters*, *40*(12), 3189–3194. https://doi.org/10.1002/grl.50571

Liguori, G., & Di Lorenzo, E. (2018). Meridional modes and increasing Pacific decadal variability under anthropogenic forcing. *Geophysical Research Letters*, *45*(2), 983–991. https://doi.org/10.1002/2017GL076548

North, G. R., Bell, T. L., Cahalan, R. F., & Moeng, F. J. (1982). Sampling errors in the estimation of empirical orthogonal functions. *Monthly Weather Review*, *110*(7), 699–706. https://doi.org/10.1175/1520-0493(1982)110<0699:SEITEO>2.0.CO;2

Pyper, B. J., & Peterman, R. M. (1998). Comparison of methods to account for autocorrelation in correlation analyses of fish data. *Canadian Journal of Fisheries and Aquatic Sciences*, *55*(9), 2127–2140. https://doi.org/10.1139/f98-104

Rogers, J. C. (1981). The north Pacific oscillation. *Journal of Climatology*, *1*(1), 39–57. https://doi.org/10.1002/joc.3370010106

Slivinski, L. C., Compo, G. P., Whitaker, J. S., Sardeshmukh, P. D., Giese, B. S., McColl, C., et al. (2019). Towards a more reliable historical reanalysis: Improvements for version 3 of the Twentieth Century Reanalysis system. *Quarterly Journal of the Royal Meteorological Society*, *145*(724), 2876–2908. https://doi.org/10.1002/qj.3598

Stuecker, M. F. (2018). Revisiting the Pacific meridional mode. *Scientific Reports*, *8*, 3216. https://doi.org/10.1038/s41598-018-21537-0

Walker, G. T., & Bliss, E. W. (1932). World weather V. *Memoirs of the Royal Meteorological Society*, *4*, 53–84.

Xie, S.-P., & Philander, S. G. H. (1994). A coupled ocean-atmosphere model of relevance to the ITCZ in the eastern Pacific. *Tellus*, *46A*, 340–350. https://doi.org/10.1034/j.1600-0870.1994.t01-1-00001.x

Yang, J.-C., Lin, X., Xie, S.-P., Zhang, Y., Kosaka, Y., & Li, Z. (2020). Synchronized tropical Pacific and extratropical variability during the past three decades. *Nature Climate Change*, *10*(5), 422–427. https://doi.org/10.1038/s41558-020-0753-9

Yang, J.-C., Zhang, Y., Lin, X., & Chang, P. (2021). Optimal growth of IPV lags AMV modulations by up to a decade. *Geophysical Research Letters*, *48*(24), e2021GL096654. https://doi.org/10.1029/2021GL096654

Zhang, Y., Xie, S.-P., Kosaka, Y., & Yang, J.-C. (2018). Pacific decadal oscillation: Tropical Pacific forcing versus internal variability. *Journal of Climate*, *31*(20), 8265–8279. https://doi.org/10.1175/JCLI-D-18-0164.1

Zhang, Y., Yu, S., Amaya, D. J., Kosaka, Y., Larson, S. M., Wang, X., et al. (2021). Pacific meridional modes without equatorial Pacific influence. *Journal of Climate*, *34*, 5285–5351. https://doi.org/10.1175/JCLI-D-20-0573.1